

Enabling LVRT Compliance of Electrolyzer Systems Using Energy Storage Technologies

Saha, Pankaj; Zhao, Weihao; Stroe, Daniel-Ioan; Iov, Florin; Munk-Nielsen, Stig

Published in:
Batteries

DOI (link to publication from Publisher):
[10.3390/batteries9110527](https://doi.org/10.3390/batteries9110527)

Creative Commons License
CC BY 4.0

Publication date:
2023

Document Version
Publisher's PDF, also known as Version of record

[Link to publication from Aalborg University](#)

Citation for published version (APA):
Saha, P., Zhao, W., Stroe, D.-I., Iov, F., & Munk-Nielsen, S. (2023). Enabling LVRT Compliance of Electrolyzer Systems Using Energy Storage Technologies. *Batteries*, 9(11), Article 527.
<https://doi.org/10.3390/batteries9110527>

General rights

Copyright and moral rights for the publications made accessible in the public portal are retained by the authors and/or other copyright owners and it is a condition of accessing publications that users recognise and abide by the legal requirements associated with these rights.

- Users may download and print one copy of any publication from the public portal for the purpose of private study or research.
- You may not further distribute the material or use it for any profit-making activity or commercial gain
- You may freely distribute the URL identifying the publication in the public portal -

Take down policy

If you believe that this document breaches copyright please contact us at vbn@aub.aau.dk providing details, and we will remove access to the work immediately and investigate your claim.

Article

Enabling LVRT Compliance of Electrolyzer Systems Using Energy Storage Technologies

Pankaj Saha , Weihao Zhao, Daniel-Ioan Stroe , Florin Iov  and Stig Munk-Nielsen 

AAU Energy, Aalborg University, 9220 Aalborg, Denmark; psa@energy.aau.dk (P.S.); wzh@energy.aau.dk (W.Z.); fi@energy.aau.dk (F.I.); smn@energy.aau.dk (S.M.-N.)

* Correspondence: dis@energy.aau.dk

Abstract: This paper presents a comprehensive techno-economic analysis of different energy storage systems (ESSs) in providing low-voltage ride-through (LVRT) support for power electronics-based electrolyzer systems. A framework for analyzing the performance of a grid-integrated electrolyzer-ESS system is developed, taking into account realistic scenarios and accurate models. The system components consist of a 500 kW alkaline electrolyzer module integrated with a medium-voltage grid and three different commercially available ESSs based on Li-ion battery, Li-ion capacitor, and supercapacitor technology, respectively. The performance of these ESSs is extensively studied for three LVRT profiles, with a primary focus on the upcoming Danish grid code. In order to perform simulation studies, the system is implemented on the MATLAB®/Simulink®-PLECS® platform. The results demonstrate that all three energy storage technologies are capable of supporting the electrolyzer systems during low-voltage abnormalities in the distribution grid. The study also reveals that the supercapacitor-based technology seems to be more appropriate, from a techno-economic perspective, for fault ride-through (FRT) compliance.

Keywords: power-to-X; electrolyzer; green hydrogen; grid code compliance; LVRT; energy storage



Citation: Saha, P.; Zhao, W.; Stroe, D.-I.; Iov, F.; Munk-Nielsen, S. Enabling LVRT Compliance of Electrolyzer Systems Using Energy Storage Technologies. *Batteries* **2023**, *9*, 527. <https://doi.org/10.3390/batteries9110527>

Academic Editor: Pascal Venet

Received: 16 September 2023

Revised: 12 October 2023

Accepted: 19 October 2023

Published: 24 October 2023



Copyright: © 2023 by the authors. Licensee MDPI, Basel, Switzerland. This article is an open access article distributed under the terms and conditions of the Creative Commons Attribution (CC BY) license (<https://creativecommons.org/licenses/by/4.0/>).

1. Introduction

With the rapid enhancement of renewable energy generation and the advancement of electrolyzer technologies, power-to-hydrogen projects are gaining significant interest in renewable energy storage as an alternative to traditional solutions, including energy storage technologies [1]. Electrolyzers produce hydrogen through water electrolysis using electricity, mainly from renewable sources [2,3]. There are some other processes used to produce hydrogen such as natural gas reforming, biomass-derived liquid reforming, microbial biomass conversion, etc. Each of these processes have their own merits and drawbacks. Furthermore, the hydrogen produced through several pathways is classified into grey, brown, blue, and green hydrogen [4]. Among these, green hydrogen generation, through water electrolysis using renewable energy, is a CO₂-neutral process [5]. The remaining hydrogen production processes involve CO₂ emissions of different quantities as a byproduct and, hence, do not comply with the clean energy criteria. The generated hydrogen is subsequently transmitted via pipeline for industrial applications and/or stored in a storage facility for later use as a fuel [6]. One of the potential applications of hydrogen fuel is the fuel-cell electric vehicle, where hydrogen combines with oxygen and generates electricity when required through reverse electrolysis [7,8].

The European Union targets a 45% GHG reduction compared to 1990 levels by 2030, and net zero emissions by 2050 [9]. Denmark has taken a leading position in implementing policies aimed at reducing greenhouse gas (GHG) emissions. It intends to reduce emissions by 70% by 2030 and achieve carbon neutrality by 2050 [10]. To achieve this, it is essential to have industrial-scale production of green hydrogen. Consequently, there is a large focus on the planning, development, and integration of large electrolyzer units into hundreds of

MW plants. Different technologies like alkaline water (ALK) electrolysis, proton exchange membrane (PEM) electrolysis, solid oxide electrolysis (SOES), and high-temperature water electrolysis can be used to produce hydrogen through electrolysis. Currently, ALK is the most cost-effective technology for producing electrolytic-grade hydrogen at around 700–800 EUR/kW. On the other hand, PEM and SOES methods are still expensive, costing around 1000–1500 EUR/kW and 2800–5600 EUR/kW, respectively [11]. At present, ALK and PEM electrolyzers are the leading technologies in the global market. In 2022, the EU installed approximately 80 MW, which is more than double the amount installed the previous year. In July of the same year, the European Commission gave the green light to provide funding worth EUR 5.4 billion to support Hy2Tech, the first hydrogen-related Important Project of Common European Interest (IPCEI) [12]. This project aims to promote hydrogen technologies, including incentives for manufacturers of electrolyzers. Denmark is constructing two energy islands that will generate green energy, including hydrogen fuel, by utilizing its abundant wind energy resources in the North and Baltic seas [13].

In order to maintain the stability and security of the power supply, new grid connection requirements are addressing specifically the installation of new electrolyzers. Besides the power quality requirements, inherent for any type of consumer connected to the electricity grid, more flexibility from such plants will be required in order to integrate them with renewable energy production, e.g., wind and solar. The security of the power supply will require these new installations to withstand large voltage drops in the electrical grid, i.e., they must remain connected to the grid in case of short-circuit events in the upstream electrical infrastructure. Typically, all consumers are disconnected from the power grid in case of a short-circuit detected in their point of connection. Then, it is immediately reconnected after the fault is cleared. Thus, a sudden disconnection of large consumer capacities in case of a short-circuit may pose challenges to power system stability and security of supply by triggering blackouts in large areas.

The electrolyzer systems have long start-up periods according to their operational state before the event. A cold start-up may take several hours, depending on technology, while a normal start-up after disconnection from the power supply may take up to one hour. Thus, following a short-circuit occurring in the transmission grid, large electrolyzer modules may be disconnected for several hours. In order to mitigate this, the new grid connection requirements are demanding that electrolyzers stay connected during the fault until it is cleared [14]. Moreover, the new criterion for the security of supply in Denmark accounts for a loss of 1 GW of electrolyzer modules [14].

The current technologies for electrolyzer systems are typically comprised of one rectification stage that directly supplies the electrolyzer stacks running at full hydrogen production [15,16]. More flexibility in hydrogen production is achieved by using controlled rectifiers with or without an additional DC-to-DC stage that enables the stacks to operate in a wider range. More advanced power conversion stages involve an active front-end rectification stage [17,18]. However, all these power conversion configurations will interrupt the power supply of the electrolyzer stacks in case of a fault in the power system.

Energy storage systems (ESSs) can be a viable solution in supporting the low-voltage ride-through (LVRT) of electrolyzer systems by providing the necessary power supply to the stack during the event while keeping the system running and ready to be reconnected to the grid when the fault is cleared. Li-ion batteries are the most popular energy storage technology. Their emerging and developed chemistries have resulted in next-generation Li-ion batteries with high energy densities, high discharge rates, enhanced cycle lives, and improved safety [19]. The supercapacitor is another promising energy storage technology considered as a potential candidate in this study due to its fast discharge capability. Unlike Li-ion battery technology, a supercapacitor stores energy as a charge double-layer without involving any chemical reactions, achieving high power density. In addition, a supercapacitor has the following advantages: rapid charging/discharging capacity, long cycle life (≥ 50 k), and a wide operating temperature range (-40 °C to 60 °C) [20]. A supercapacitor is ideal for applications that require high currents for short periods, typically a few minutes,

due to its rapid charge delivery capacity. Similarly, an Li-ion capacitor is a hybrid energy storage system that combines, in a trade-off solution, electric-double layer-based supercapacitor technology and charge intercalation-based Li-ion battery technology. Such an energy storage system combines the advantages of both the technologies mentioned above, including high power density, high energy density, long cycle life, and a wide operating temperature range [21].

A number of studies have proposed in the past to utilize batteries with renewable-based energy systems such as wind and solar PV to comply with grid codes for LVRT [22–27]. In all cases, depending on the rating of these renewable sources, the ESS must have a high power density to supply a large amount of power for a short duration of time, i.e., up to a couple of seconds. The same approach of integrating ESS into the power conversion stages may be used to achieve the new LVRT requirements for electrolyzer systems. However, the necessary power and energy that needs to be delivered by ESSs for these tens of MW systems may be very different compared to renewable-based ones. Currently, there is no study in the public domain that evaluates the necessary power and energy required by an electrolyzer unit to comply with the upcoming LVRT requirements. Moreover, as various ESS technologies are available on the market, guidelines and recommendations for their usage in connection with electrolyzer units are missing. Hence, this paper aims to perform a techno-economic analysis of three energy storage technologies, i.e., lithium-ion batteries, greenlithium-ion capacitors, and greensupercapacitors, for their potential to enable the upcoming LVRT requirements of large electrolyzer systems.

The main contributions of this paper are as follows: (i) a methodology for sizing the considered ESS technologies is proposed, including the configuration of the cells to comply with any LVRT requirements; (ii) the technical performance of the ESS embedded into the electrolyzer unit for LVRT compliance is assessed through relevant simulation studies considering three voltage profiles, including the upcoming Danish grid code requirements; and (iii) a techno-economic assessment of the considered ES technologies is conducted and guidelines for future deployment in real installations are provided.

The rest of the paper is organized into five sections. Section 2 outlines the overall system design. Section 3 provides details on three different energy storage technologies. Section 4 presents simulation results and discussion. Finally, Section 5 concludes the paper.

2. Characterization of System

2.1. Electrolyzer Module

Following the approach described in [18], the system's scope comprises of a 500 kW electrolyzer and an ESS connected to the medium voltage distribution system, as shown in Figure 1.

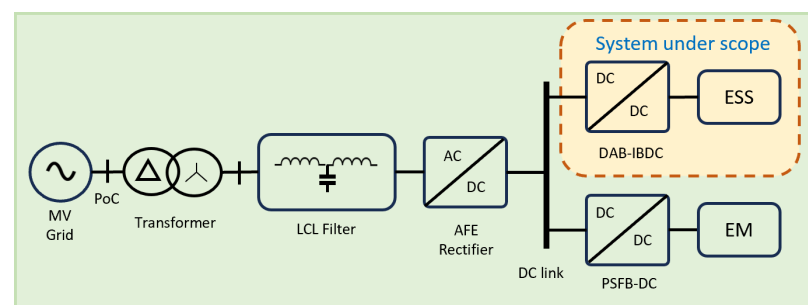


Figure 1. Block diagram of a grid-integrated electrolyzer module with embedded energy storage system (AFE: active front-end; DAB-IBDC: dual-active-bridge isolated bidirectional DC-DC converter; PSFB-DC: phase-shift full-bridge DC-DC converter; EM: electrolyzer module; and ESS—energy storage system).

A 10 kV connection, as a typical voltage level in the Danish distribution system, is considered. A step-down transformer will provide a 2.5 kV line-to-line feed for the

active front-end (AFE) rectifier. An LCL filter designed to mitigate the high harmonic content is also included. The AFE rectifier provides a 6 kV voltage for the common DC link circuit. Both the electrolyzer and ESS are connected to this common DC-link circuit through a phase-shift full-bridge DC-DC converter (PSFB-DC) and a dual-active-bridge (DAB) isolated bidirectional DC-DC converter (IBDC), respectively.

A classical dq control is used for the rectifier stage as described in [18]. The d-axis comprises an inner current control and an outer DC-link voltage control loop, respectively. Similarly, an inner current control loop and the reactive power outer control loop are present in the q-axis. The electrolyzer module current is controlled using a standard current control loop, as described in [18]. The charging and discharging currents for the battery are also controlled using the same approach as for the electrolyzer.

During normal operation, i.e., supply voltage within ± 0.1 p.u., the PSBF converter supplies the current and voltage to the electrolyzer module required for producing hydrogen while the ESS remains in the idling mode. As a short-circuit occurs in the distribution grid, the DC-link voltage will drop significantly according to the voltage level measured in the point-of-connection (PoC), and the power supply in the common DC-link circuit will be handled by the ESS.

2.2. LVRT Profiles

Three voltage profiles for the LVRT are considered for this analysis, i.e., the upcoming Danish grid code [14], the Standard grid code [27], and the upcoming German grid code [28], as shown in Figure 2. The upcoming Danish grid code outlines the requirements for large Power-to-X systems connected to transmission networks. The regulation capabilities of the Danish grid code consists of a 100% voltage dip for 150 ms during a fault, followed by a 35% voltage recovery (i.e., a 65% voltage dip for another 550 ms). The voltage then gradually ramps up to 90% of its normal operating condition within 800ms. Similarly, the Standard grid code consists of a 100% voltage dip for 150 ms during a fault, followed by gradual voltage ramps up to 90% of its normal operating condition in the next 1.5 s. The upcoming German grid code, on the other hand, takes 3 s to ramp up to 90% of normal operating conditions. The considered recovery times for the grid voltage are very similar to the LVRT requirements applied to renewable generation, e.g., wind and solar PV plants [27,29].

In order to comply with LVRT requirements, the electrolyzer system must fulfill the following conditions: (i) It must operate normally for voltage levels down to 0.9 p.u., i.e., Area A. (ii) It must stay connected to the grid for voltage levels above the LVRT profiles Area B. In the current grid codes, it is not specified what the operational state of the electrolyzer in this area shall be. However, the start-up of the electrolyzer may take up to 1 h, and most of the technologies may ramp down to about 0.1 p.u. hydrogen production in several seconds. Thus, an additional energy source shall provide the necessary power for keeping the electrolyzer running until the fault is cleared. (iii) The entire electrolyzer system may disconnect for voltage levels below the LVRT profile, i.e., Area C [30].

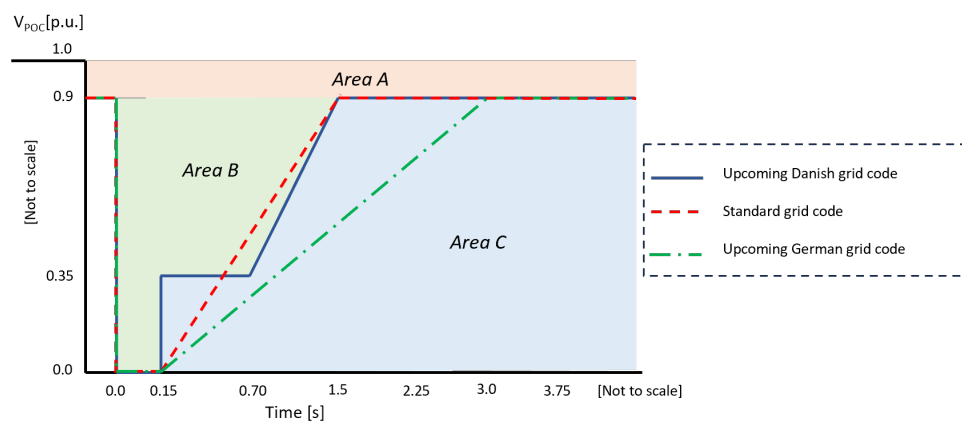


Figure 2. LVRT profiles in point-of-connection (PoC).

2.3. Methodology for ESS Sizing

This section proposes a methodology for sizing the ESSs' power and energy as well as the series and parallel configurations of the cells to ensure a continuous operation of the electrolyzer stack during LVRT. Assuming that there are no losses in the subsystems between the ESS and electrolyzer stack (as shown in Figure 1), the power and voltage rating of the ESS must comply with the electrolyzer and ESS-connected DC-DC converter ratings, respectively. A sizing procedure for the ESS according to the required power and the duration of the fault is given in the following paragraphs.

Step 1: For a given time duration (T_d) and the rated power (P_r), the total energy required by the electrolyzer stack can be calculated as:

$$E_{wh} = \frac{P_r T_d}{3600} \quad (1)$$

where E_{Wh} is the energy in watt-hours, and T_d is the time duration in seconds during which the ESS needs to supply power to the electrolyzer.

Step 2: The required number of series-connected cells (N_s) of the ESS is:

$$N_s = \frac{V_r}{V_{cell}} \quad (2)$$

where V_r is the rated voltage of the electrolyzer, and V_{cell} is the nominal voltage of a unit cell of the ESS.

Step 3: The number of parallel strings (N_p) can be calculated as:

$$N_p = \frac{E_{wh}}{V_r C_{Ah}} \quad (3)$$

where C_{Ah} is the unit cell capacity in ampere-hour. Essentially, the number of parallel strings defines the discharge current rate of the cells. Thus, if the obtained parallel strings value does not satisfy the cell's maximum discharge current limit, the value of N_p must be re-calculated following the subsequent steps. This will result in an over-sized ESS with plenty of energy remaining in the storage system even after fulfilling the power demand for the time duration T_d .

Step 4: The load current of the electrolyzer system is given by:

$$I_l = \frac{P_r}{V_r} \quad (4)$$

Step 5: For a given maximum continuous discharge current (I_{maxC}) of the cell, the number of parallel strings of the ESS can be calculated as:

$$N_p = \frac{I_l}{I_{maxC}} \quad (5)$$

The flow chart of the ESS sizing methodology is displayed in Figure 3. The results of the ESS sizing for the three considered energy storage technologies using the proposed methodology are presented in Section 4.

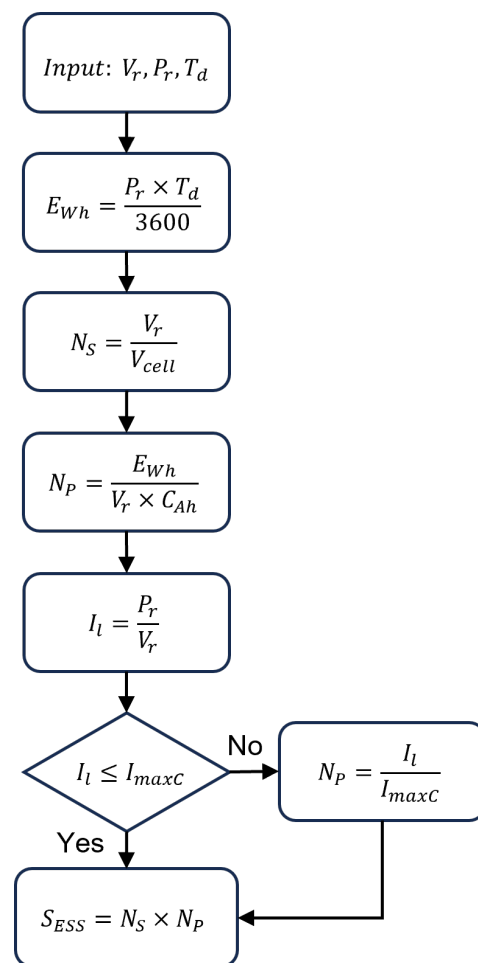


Figure 3. Flow chart for sizing ESSs to pinkenable LVRT of electrolyzer.

3. ESS Technologies

This section presents the mathematical models for the considered ESS technologies in this analysis.

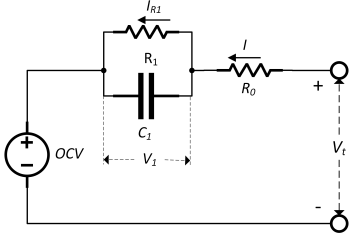
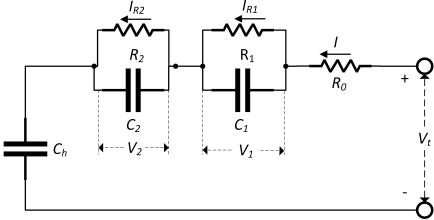
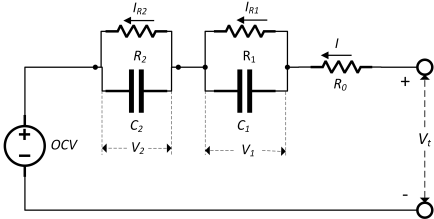
3.1. Lithium-Ion Batteries

This study considers a 180 Ah commercial Li-ion battery made of a lithium iron phosphate (LFP) cathode and a graphite anode. The detailed specifications of the considered Li-ion battery cell are listed in Table 1. The Thevenin equivalent circuit model (ECM) used for dynamic studies and corresponding mathematical equations are listed in Table 2. The ECM consists of a DC voltage source capturing the OCV as a function of SOC, an equivalent series resistance (R_0) capturing the Ohmic voltage drop across the cell and a parallel RC branch (R_1C_1) characterizing the cell's internal charge transfer and diffusion resistances.

Table 1. Technical specifications of selected ESS cells.

Parameter	Li-Ion Battery	Li-Ion Capacitor	Supercapacitor
Nominal voltage [V]	3.2	3	2
Voltage range [V]	2.5–3.65	2.2–3.8	1.35–2.7
Capacity [Ah]	180	0.93	1.125
Max. continuous current [A]	720	100	210
Specific power [W/kg]	205	4×10^3	5.9×10^3
Specific energy [Wh/kg]	102	24	6
Mass [kg]	5.6	0.11	0.51
Volume [m ³]	36×10^{-4}	1.11×10^{-4}	3.95×10^{-4}

Table 2. Electrical equivalent circuit models.

Energy Storage Technology	Equivalent Circuit Model	Mathematical Representation
Li-ion battery		$\dot{SOC} = -I(3600C_{Ah})^{-1}$ $\dot{V}_1 = -(R_1C_1)^{-1} + IC_1^{-1}$ $V_t = OCV(SOC) + V_1 + IR_0$
Supercapacitor		$\dot{V}_h = IC_h^{-1}$ $\dot{V}_1 = -(R_1C_1)^{-1} + IC_1^{-1}$ $\dot{V}_2 = -(R_2C_2)^{-1} + IC_2^{-1}$ $V_t = V_h + V_1 + V_2 + IR_0$
Li-ion capacitor		$\dot{SOC} = -I(3600C_{Ah})^{-1}$ $\dot{V}_1 = -(R_1C_1)^{-1} + IC_1^{-1}$ $\dot{V}_2 = -(R_2C_2)^{-1} + IC_2^{-1}$ $V_t = OCV(SOC) + V_1 + V_2 + IR_0$

3.2. Supercapacitors

A commercially available 3000F supercapacitor (Maxwell BCAP3000) was considered to study the effectiveness of this technology in supporting the electrolyzer unit. To simulate the electrical dynamics of the supercapacitor, a 3rd-order ECM of the system has been adopted from [31]. The model consists of a capacitor (C_h), a resistor (R_{esr}), and two parallel RC branches (R_1C_1, R_2C_2). Table 2 contains the ECM of the supercapacitor and the corresponding mathematical equations. The voltage across the capacitor C_h denoted by V_h , V_1 denotes voltage across the R_1C_1 branch, V_2 denotes voltage across the R_2C_2 branch, V_t denotes voltage across the output terminal of the supercapacitor, and I denotes current flow through the supercapacitor.

3.3. Lithium-Ion Capacitors

In this paper, a commercially available 2100F (Musashi CLE2100S1B) Li-ion capacitor was considered for further studies. A 2nd-order ECM of the cell was adopted from [32] to simulate the electrical dynamic response of the Li-ion capacitor. The model consists of a DC voltage source capturing the OCV as a function of SOC, an equivalent series resistance (R_{esr}), and two parallel RC branches (R_1C_1, R_2C_2). The Li-ion capacitor ECM and the corresponding mathematical equations can be seen in Table 2, where C_{Ah} denotes capacity in ampere-hours (Ah), V_1 denotes voltage drop across the R_1C_1 branch, V_2 denotes voltage drop across the R_2C_2 branch, V_t denotes output terminal voltage, and I denotes input current ('+'/'-': discharge/charge) of the cell.

4. Results and Discussion

A model-based design approach was used to implement the electrolyzer system, including the ESS technologies, as described in Figure 1. Thus, all power converters, including semiconductor devices, were implemented in PLECS®green (Blockset 4.7.5) while the electrolyzer stack, the ESS technologies in scope, and all the controls were

implemented as MATLAB®/Simulink®green (R2023a) models outside PLECS®. All system design parameters and tuning procedures for the AFE, the DC/DC converter for supplying the electrolyzer, and the electrolyzer model were according to [18], while the three ESS models, including controls, were implemented additionally as part of this study. The technical performance of the considered ESS technologies is evaluated for the LVRT profiles in point-of-connection (PoC), as shown in Figure 1. Thus, the study consists of case studies. However, for the sake of simplicity, only the ESS performance under the upcoming Danish grid code is discussed in detail, with brief conclusions drawn for the remaining cases.

By using the sizing methodology described in Section 2.3, the ESS technologies were designed for an LVRT event of 1.5 s, as illustrated in Figure 2. According to the system design parameters outlined in [18], the electrolyzer stack has a rated power of 500 kW, and the DC-link voltage is 6 kV. So, the electrolyzer must be supplied by an ESS with a capacity of $(500 \text{ kW} \times 1.5 \text{ s}) \div 3600 = 208.34 \text{ Wh}$. Considering the voltage conversion ratio of the DC-DC boost converter is 6.66, the rated voltage of the ESS was calculated to be 900 V. Thus, all three ESS technologies were designed to meet both the power and energy criteria of the electrolyzer.

Table 3 shows the results of the sizing procedure in terms of the minimum number of cells required in series and in parallel, as well as the corresponding energy of the entire energy storage module. Unlike the LVRT events of 1.5 s, the electrolyzer must be supplied by an ESS with a capacity of 416.7 Wh for the case of extended grid code where the LVRT event lasts for 3 s. However, it is worth noting that all ESS sizes identified (in Table 3) can support all the considered LVRT events under the Danish grid code, Standard grid code, and German grid code.

Table 3. Sizing of energy storage system.

Technology	N_s	N_p	Energy Capacity [kWh]
Li-ion battery	288	1	162.4
Li-ion capacitor	300	6	5.022
Supercapacitor	450	3	3.037

4.1. AFE Response during LVRT

This subsection presents the dynamic response of several variables in the system during LVRT, the voltage and current responses on the grid side, along with the corresponding 6 kV common DC-link voltage response.

To demonstrate the system's performance, an LVRT profile is introduced in the grid voltage at $t = 0.1 \text{ s}$. Figure 4a depicts the 100% voltage dip at the grid side, while Figure 4b,c illustrate the corresponding grid current and DC-link voltage variations.

Notably, the DC link voltage deviation is less than 2% of its normal voltage during the 100% grid voltage dip. When the grid voltage drops below 90%, the ESS switches from idling mode to discharging mode and begins to supply the electrolyzer via the common DC-link. Once the voltage is restored to 90% of its normal value, the ESS switches back to idling mode from discharging mode and stops supplying power to the DC link, as depicted in Figure 4. It is evident that the ESSs effectively maintained the DC-link voltage during abnormal grid voltages. The AFE response was identical for all considered ESSs technologies.

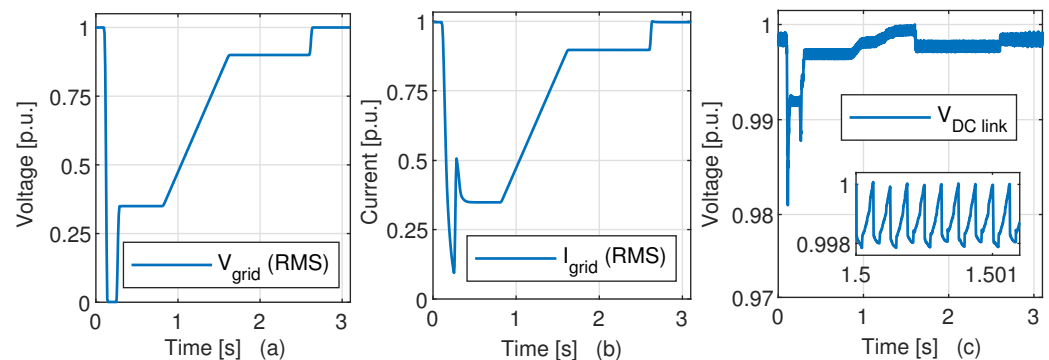


Figure 4. Grid (a) voltage, (b) current, and (c) DC-link voltage responses.

4.2. Electrolyzer Response during LVRT

This section focuses on the response of the electrolyzer module under the operating conditions shown in Figure 4. It is assumed that the electrolyzer will not change its operational state during the LVRT, and hence it will continue to operate at its nominal hydrogen production rate. The electrolyzer input current, voltage, and power are shown in Figure 5a–c. Even with a 100% grid voltage dip, the electrolyzer input current only drops by 0.005 p.u. of its normal operating value.

A ± 0.025 p.u. ripple in voltage is due to the switchings in the DC/DC converter, as expected. Consequently, due to the filters in the converter, a smaller ripple (less than ± 0.001 p.u.) can be observed in the supplied current to the electrolyzer. Regardless of ESS technology used, the power supply of the electrolyzer is maintained within a deviation of less than 0.02 p.u. in all test cases.

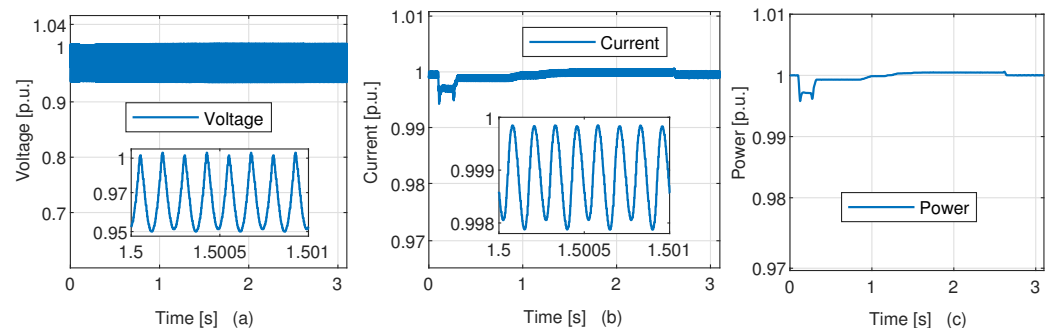


Figure 5. Electrolyzer (a) voltage, (b) current, and (c) power responses during the grid code compliance by the energy storage systems.

4.3. ESS Response during LVRT

This section compares the LVRT performance of the three considered energy storage technologies. The ECM of the three ESSs discussed in Section 3 have been implemented. Three grid–electrolyzer–ESS system models were implemented for the three selected energy storage technologies, using the sizes listed in Table 3. Figure 6 illustrates the dynamic response of three ESSs during an LVRT event as per the upcoming Danish Grid Code.

At the beginning of the LVRT event, all three ESSs experience the maximum discharge current, causing a sudden drop in their terminal voltage due to the presence of Ohmic resistance in the storage devices. The varying starting voltages of the ESSs in Figure 6a are a result of their different maximum voltage levels as listed in Table 4 at 100% SOC. As the grid voltage recovers, the current demand to supply the electrolyzer decreases. Thus, the discharge current value decreases to zero when the grid voltage is restored at 90% of normal operating voltage. Figure 6c shows that the SOC of the ESSs reduces steadily as the electrolyzer consumes power from them. When the grid power is restored to 90% of its normal operating condition after 1.5 s, the ESSs stop providing power and are disconnected

from the electrolyzer; hence, the SOC remains constant until the end of the simulation period. The supercapacitor-based ESS experiences the highest SOC drop ($>6\%$), and the Li-ion battery-based ESS shows the lowest one ($<1\%$) due to the high energy/capacity of this technology. Based on the energy required to comply with the grid code, the supercapacitor-based ESS is the least oversized in terms of energy capacity (as listed in Table 3), and the Li-ion battery-based ESS is the largest.

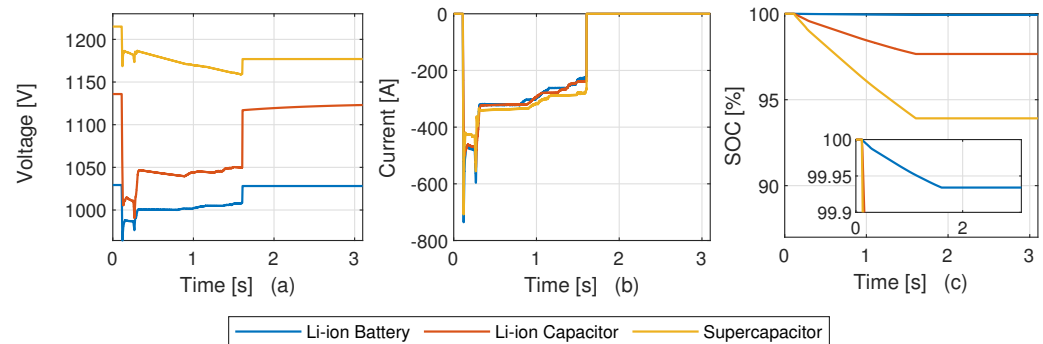


Figure 6. Energy storage systems (a) voltage, (b) current, and (c) SOC response.

Table 4. Comparative analysis of different energy storage technologies.

Parameter	Li-Ion Battery	Li-Ion Capacitor	Supercapacitor
Price (\$/kWh)	300	37,167	2500
Installation cost (\$)	48,720	186,650	7600
Mass (kg)	1612.8	198	688.5
Volume (m ³)	1.03	0.2	0.54
Max. backup duration (s)	1160.8	36.15	21.86
Cycle life (cycles)	~2000	~300,000	~1000,000

Since the minimum number of series and parallel cells required for riding the low voltage fault is the same, as listed in Table 3, similar results have been obtained for the other two LVRT profiles, i.e., the Standard grid code and the upcoming German grid code. Figure 7 presents the SOC drop values for each ESS and the considered LVRT profiles. For all three energy storage systems, the largest drop in state of charge occurred for the German grid code scenario, which has the longest fault duration of 3 s. In addition, the supercapacitor-based energy storage technology exhibits the highest SOC drop for all the cases, which is consistent with the energy capacity of the storage module.

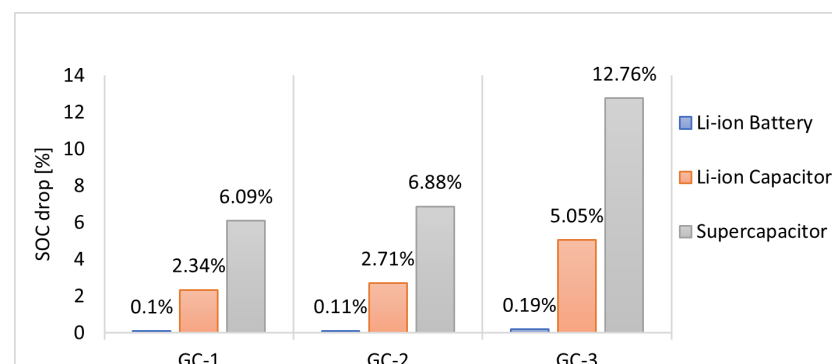


Figure 7. SOC drop experienced by the energy storage technologies for the three different grid codes (GC-1: Upcoming Danish grid code; GC-2: Standard grid code; GC-3: Upcoming German grid code).

4.4. Techno-Economic Analysis

From a techno-economic perspective, a comprehensive analysis of the considered ESSs is conducted to determine the best storage technology for supporting the electrolyzer module. Four key performance parameters, namely installation cost, weight, backup time, and lifetime, are considered in the assessment. The installation cost of the ESSs is calculated using the unit price of the Li-ion battery, Li-ion capacitor, and supercapacitor, which are 300 USD/kWh, 37167 USD/kWh, and 2500 USD/kWh, respectively [33,34]. The backup time metric defines the duration for which a fully charged ESS can meet the power demand of the electrolyzer module. The analysis is performed for the ESS size derived in Table 3, and the results are presented in Table 4. The analysis shows that the supercapacitor is both technically and economically feasible for LVRT support of the electrolyzer module. Clearly, the Supercapacitor-based technology outperforms both the Li-ion battery and Li-ion capacitor technologies in installation cost and cycle life. Based on the remaining performance parameters in Table 4, it is evident that the supercapacitor is a good trade-off among the three selected storage technologies for LVRT support. Consideration of the impact of the high discharge current on the ESSs' state of health in techno-economic analysis can be a direction of future studies.

5. Conclusions

In this work, we thoroughly examine the effectiveness of various energy storage technologies in complying with grid code standards for LVRT in electrolyzer-based pink systems. A grid-integrated alkaline electrolyzer module–ESS framework was designed to conduct simulation studies using the MATLAB®/Simulink®-PLECS® platform. The framework includes an MV grid of 10 kV, an alkaline electrolyzer of 500 kW, and energy storage systems. The study focuses on commercially available energy storage technologies such as Li-ion batteries, Li-ion capacitors, and supercapacitors under three different grid codes, primarily focusing on the upcoming Danish grid code. Firstly, we have proposed a methodology for sizing the ESSs, in terms of power and energy to satisfy the system's current and voltage constraints. The simulation results indicate that (1) all energy storage systems are capable of supporting the electrolyzer module in withstanding voltage dips at the grid side; (2) during LVRT support, the ESSs can maintain the DC link voltage at its normal operating voltage with a deviation of less than 0.02 p.u.; (3) the operating power deviation for the electrolyzer modules is limited to within 0.005 p.u. of its normal operating power; and (4) from the techno-economic perspective, it is evident that supercapacitor-based energy storage technology is the most optimal solution among the three energy storage technologies. Furthermore, it has to be highlighted that even for the most energy-demanding LVRT scenario, there is between 87% and 99% available energy (depending on the ESS technology) at the end of the grid event. Thus, the use of the ESS for additional services (besides LVRT compliance) should be investigated to speed up the return on the investment. The present study can further extend in the following directions: (i) consideration of the impact of high C-rate on the state of health of the ESS technologies while assessing the techno-economic performance and (ii) analysis of the system dynamic response during asymmetrical grid faults.

Author Contributions: Conceptualization, P.S., W.Z., D.-I.S. and F.I.; Methodology, P.S., D.-I.S. and F.I.; Resources, W.Z., D.-I.S. and F.I.; Investigation, P.S., D.-I.S. and F.I.; Writing—original draft, P.S.; Writing—review and editing, D.-I.S. and F.I.; Supervision, D.-I.S., F.I. and S.M.-N. All authors have read and agreed to the published version of the manuscript.

Funding: The authors acknowledge the financial support through EUDP 64019-00114 SENSE, REACTRF-21-0026 “Center for Green Energy and Sector Coupling” and “PtX Converter” projects.

Acknowledgments: This research is part of the SENSE—Sustainable Energy Systems project—which is supported by the Energy Technology Development and Demonstration Program (EUDP), Denmark, under grant number 64019-00114.

Conflicts of Interest: The authors declare that they have no known competing financial interests or personal relationships that could have appeared to influence the work reported in this paper.

References

1. Agency, I.R.E. What Are the Latest Trends in Renewable Energy? Available online: <https://www.irena.org/Data/View-data-by-topic/Capacity-and-Generation/Statistics-Time-Series> (accessed on 2 September 2023).
2. Mazzeo, D.; Herdem, M.S.; Matera, N.; Wen, J.Z. Green hydrogen production: Analysis for different single or combined large-scale photovoltaic and wind renewable systems. *Renew. Energy* **2022**, *200*, 360–378. [\[CrossRef\]](#)
3. Navarro, R.; Sanchez-Sanchez, M.; Alvarez-Galvan, M.; Del Valle, F.; Fierro, J. Hydrogen production from renewable sources: Biomass and photocatalytic opportunities. *Energy Environ. Sci.* **2009**, *2*, 35–54. [\[CrossRef\]](#)
4. Dawood, F.; Anda, M.; Shafiullah, G. Hydrogen production for energy: An overview. *Int. J. Hydrogen Energy* **2020**, *45*, 3847–3869. [\[CrossRef\]](#)
5. Kumar, S.S.; Lim, H. An overview of water electrolysis technologies for green hydrogen production. *Energy Rep.* **2022**, *8*, 13793–13813. [\[CrossRef\]](#)
6. Felseghi, R.A.; Carcadea, E.; Raboaca, M.S.; Trufin, C.N.; Filote, C. Hydrogen fuel cell technology for the sustainable future of stationary applications. *Energies* **2019**, *12*, 4593. [\[CrossRef\]](#)
7. Aminudin, M.; Kamarudin, S.; Lim, B.; Majilan, E.; Masdar, M.; Shaari, N. An overview: Current progress on hydrogen fuel cell vehicles. *Int. J. Hydrogen Energy* **2023**, *48*, 4371–4388. [\[CrossRef\]](#)
8. Sharma, S.; Ghoshal, S.K. Hydrogen the future transportation fuel: From production to applications. *Renew. Sustain. Energy Rev.* **2015**, *43*, 1151–1158. [\[CrossRef\]](#)
9. European Commission. Climate Neutrality, 2050 Long-Term Strategy. Available online: <https://climate.ec.europa.eu/eu-action/climate-strategies-targets/2050-long-term-strategy-en> (accessed on 10 September 2023).
10. European Commission. Denmark’s Long-Term Strategy—European Commission. Available online: <https://ec.europa.eu/clima/sites/lts/lts-dk-en.pdf> (accessed on 10 September 2023).
11. Younas, M.; Shafique, S.; Hafeez, A.; Javed, F.; Rehman, F. An overview of hydrogen production: Current status, potential, and challenges. *Fuel* **2022**, *316*, 123317. [\[CrossRef\]](#)
12. European Commission. State Aid: Commission Approves up to €5.4 Billion of Public Support by Fifteen MEMBER States for an Important Project of Common European Interest in the Hydrogen Technology Value Chain. Available online: <https://ec.europa.eu/commission/presscorner/detail/en/ip-22-4544> (accessed on 10 September 2023).
13. Denmark’s Energy Islands. Available online: <https://ens.dk/en/our-responsibilities/energy-islands/denmarks-energy-islands> (accessed on 10 September 2023).
14. ENERGINET. Connection Requirements in Relation to Large PTX Systems to Transmission Networks. Available online: <https://en.energinet.dk/Electricity/Rules-and-Regulations/Regulations-for-grid-connection/> (accessed on 10 September 2023).
15. Guilbert, D.; Collura, S.M.; Scipioni, A. DC/DC converter topologies for electrolyzers: State-of-the-art and remaining key issues. *Int. J. Hydrogen Energy* **2017**, *42*, 23966–23985. [\[CrossRef\]](#)
16. Yodwong, B.; Guilbert, D.; Phattanasak, M.; Kaewmanee, W.; Hinaje, M.; Vitale, G. AC-DC converters for electrolyzer applications: State of the art and future challenges. *Electronics* **2020**, *9*, 912. [\[CrossRef\]](#)
17. Chen, M.; Chou, S.F.; Blaabjerg, F.; Davari, P. Overview of power electronic converter topologies enabling large-scale hydrogen production via water electrolysis. *Appl. Sci.* **2022**, *12*, 1906. [\[CrossRef\]](#)
18. Zhao, W.; Nielsen, M.R.; Kjær, M.; Iov, F.; Nielsen, S.M. Grid integration of a 500 kW alkaline electrolyzer system for harmonic analysis and robust control. *E-Prime Electr. Eng. Electron. Energy* **2023**, *5*, 100217. [\[CrossRef\]](#)
19. Kim, T.; Song, W.; Son, D.Y.; Ono, L.K.; Qi, Y. Lithium-ion batteries: Outlook on present, future, and hybridized technologies. *J. Mater. Chem. A* **2019**, *7*, 2942–2964. [\[CrossRef\]](#)
20. Saha, P.; Dey, S.; Khanra, M. Modeling and state-of-charge estimation of supercapacitor considering leakage effect. *IEEE Trans. Ind. Electron.* **2019**, *67*, 350–357. [\[CrossRef\]](#)
21. Soltani, M.; Beheshti, S.H. A comprehensive review of li-ion capacitor: development, modelling, thermal management applications. *J. Energy Storage* **2021**, *34*, 102019. [\[CrossRef\]](#)
22. Hazari, M.R.; Jahan, E.; Mannan, M.A.; Tamura, J. Coordinated control scheme of battery storage system to augment LVRT capability of SCIG-based wind turbines and frequency regulation of hybrid power system. *Electronics* **2020**, *9*, 239. [\[CrossRef\]](#)
23. Gayathri, T.; Ananth, D.; Kumar, G.N.; Sivanagaraju, G. Enhancement in dynamic and LVRT behaviour of an EFOC controlled DFIG with integrated Battery Energy Storage System. In Proceedings of the 2013 Annual IEEE India Conference (INDICON), Mumbai, India, 13–15 December 2013; pp. 1–6.
24. Huy, T.N.; Le Hanh, D.; Takano, H.; Duc, T.N. Cooperative LVRT control for protecting PMSG-based WTGs using battery energy storage system. *Energy Rep.* **2023**, *9*, 590–598.
25. Jin, C.; Wang, P. Enhancement of low voltage ride-through capability for wind turbine driven DFIG with active crowbar and battery energy storage system. In Proceedings of the IEEE PES General Meeting, Minneapolis, MN, USA, 25–29 July 2010; pp. 1–8.
26. Kalyan, R.; Murali, V.; Pitchaimuthu, R. Coordinate Control of Grid Power, Battery SoC and LVRT Protection in Single VSC Tied DFIG. *Distrib. Gener. Altern. Energy J.* **2022**, *37*, 587–608. [\[CrossRef\]](#)

27. Rai, R.; Singh, B. Converter Control During Low Voltage Ride Through Operation for Grid-Interfaced Solar PV Battery Assisted System. *IEEE Trans. Ind. Electron.* **2022**, *70*, 9181–9191. [\[CrossRef\]](#)
28. Raphael, B.; Johannes, W.; Volker, S.; Christian, S.; Stanko, J., Dr.; Hartmut, P., Dr. Requirements for Power-to-Gas Units. In Proceedings of the 22nd Wind and Solar Integration Workshop, Copenhagen, Denmark, 26–28 September 2023.
29. Kabsha, M.M.; Rather, Z.H. Advanced LVRT control scheme for offshore wind power plant. *IEEE Trans. Power Deliv.* **2021**, *36*, 3893–3902. [\[CrossRef\]](#)
30. Energynet. Regulations for Grid Connection. Available online: <https://en.energinet.dk/Electricity/Rules-and-Regulations/Regulations-for-grid-connection/> (accessed on 2 September 2023).
31. Bansal, S.; Nambisan, P.; Saha, P.; Khanra, M. Effect of supercapacitor modelling and unit cell capacitance selection towards economic sizing of energy storage system in electric vehicle. *J. Energy Storage* **2022**, *51*, 104517. [\[CrossRef\]](#)
32. Pankaj, S.; Mahdi, S.; Stig, M.N.; Daniel-Ioan, S. A Model Predictive Control Approach for Lithium-ion Capacitor Optimal Charging. In Proceedings of the 2023 The 25th European Conference on Power Electronics and Applications (EPE'23 ECCE Europe), Aalborg, Denmark, 4–8 September 2023; pp. 1–6.
33. BloombergNEF (BNEF). Near-Term Lithium-Ion Battery Cell and Pack Price Forecast. Available online: <https://about.bnef.com/blog/top-10-energy-storage-trends-in-2023/> (accessed on 2 September 2023).
34. Roy, P.K.S.; Karayaka, H.B.; He, J.; Yu, Y.H. Economic comparison between battery and supercapacitor for hourly dispatching wave energy converter power. In Proceedings of the 2020 52nd North American Power Symposium (NAPS), Tempe, AZ, USA, 11–13 April 2021; pp. 1–6.

Disclaimer/Publisher's Note: The statements, opinions and data contained in all publications are solely those of the individual author(s) and contributor(s) and not of MDPI and/or the editor(s). MDPI and/or the editor(s) disclaim responsibility for any injury to people or property resulting from any ideas, methods, instructions or products referred to in the content.